Computers and Concrete, Vol. 9, No. 6 (2012) 403-426
DOI: http://dx.doi.org/10.12989/cac.2012.9.6.403

Structural behaviour of tapered concrete-filled steel composite (TCFSC) columns subjected to eccentric loading

Alireza Bahrami*, Wan Hamidon Wan Badaruzzaman and Siti Aminah Osman

Department of Civil and Structural Engineering, Universiti Kebangsaan Malaysia, Bangi, Selangor, Malaysia

(Received February 25, 2011, Revised July 11, 2011, Accepted August 21, 2011)

Abstract. This paper deals with the structural behaviour of tapered concrete-filled steel composite (TCFSC) columns under eccentric loading. Finite element software LUSAS is used to perform the nonlinear analyses to predict the structural behaviour of the columns. Results from the finite element modelling and existing experimental test are compared to verify the accuracy of the modelling. It is demonstrated that they correlate reasonably well with each other; therefore, the proposed finite element modelling is absolutely accurate to predict the structural behaviour of the columns. Nonlinear analyses are carried out to investigate the behaviour of the columns where the main parameters are: (1) tapered angle (from 0^o to 2.75^o); (2) steel wall thickness (from 3 mm to 4 mm); (3) load eccentricity (15 mm and 30 mm); (4) L/H ratio (from 10.67 to 17.33); (5) concrete compressive strength (from 30 MPa to 60 MPa); (6) steel yield stress (from 250 MPa to 495 MPa). Results are depicted in the form of load versus mid-height deflection plots. Effects of various tapered angles, steel wall thicknesses, and L/H ratios on the ultimate load capacity, ductility and stiffness of the columns are studied. Effects of different load eccentricities, concrete compressive strengths and steel yield stresses on the ultimate load capacity of the columns are also examined. It is concluded from the study that the parameters considerably influence the structural behaviour of the columns.

Keywords: tapered concrete-filled steel composite column; eccentric loading; finite element; nonlinear analysis; ultimate load capacity; ductility; stiffness; concrete compressive strength; steel yield stress.

1. Introduction

Concrete-filled steel composite (CFSC) columns have demonstrated many structural benefits over steel and reinforced concrete columns such as high ductility, large strength and high stiffness which can be attributed to the composite action between their main materials, steel and concrete. These benefits of the CFSC columns have resulted in their expanding use in modern civil projects throughout the world. Many studies have been conducted on the behaviour of these columns. Uy (1998b) examined effects of different materials and geometric properties on the strength and ductility of concrete-filled steel box columns. Effects of cross-sectional shapes, width-to-thickness ratios, and stiffening arrangements on the ultimate strength, stiffness and ductility of concrete-filled steel columns have been experimentally investigated by Huang *et al.* (2002). Han and Yao (2003)

* Corresponding author, Ph.D. Student, E-mail: bahrami_a_r@yahoo.com

assessed the load-deformation behaviour of concrete-filled hollow structural steel columns with the steel tubes under pre-load. Liu and Gho (2005) tested 26 high-strength rectangular concrete-filled steel tubular columns to evaluate their axial load behaviour. Ellobody and Young (2006a) presented effects of cross-section geometry and concrete strength on the behaviour and strength of concrete-filled cold-formed stainless steel tube columns. Liu (2006) reported an experimental and analytical investigation on the behaviour of eccentrically loaded high-strength rectangular concrete-filled steel tubular columns. Tao *et al.* (2007) carried out experimental tests on the behaviour of concrete-filled stiffened thin-walled steel tubular columns. Tests on stainless steel concrete-filled columns with different concrete compressive strengths were done by Lam and Gardner (2008). A method was presented by Huang *et al.* (2008) to estimate the ultimate strength of rectangular concrete-filled steel tubular stub columns under axial compression. The ultimate strength of the concrete core was determined by using the conception of the effective lateral confining pressure and a failure criterion of concrete under true triaxial compression. Dabaon *et al.* (2009) studied stiffened and unstiffened concrete-filled stainless steel tubular columns to reveal the confinement evaluation of concrete in the columns. Tests on rectangular concrete-filled steel tubular columns were performed by Yang and Han (2009). The columns were axially loaded on a partially stressed cross-sectional area. Starossek *et al.* (2010) assessed the force transfer by natural bond or by mechanical shear connecters and the interaction between the steel tube and concrete core of concrete-filled steel tube columns. Effects of tab stiffeners on the bond and compressive strengths of concrete-filled thin-walled steel tubes were reported by Petrus *et al.* (2010). Dai and Lam (2010) examined axial compressive behaviour of concrete-filled elliptical steel columns. Bahrami *et al.* (2011) studied slender CFSC columns to investigate and develop different shapes and number of cold-formed steel sheeting stiffeners with various thicknesses of cold-formed steel sheets and also evaluate their effects on the behaviour of the columns.

Structural behaviour of tapered concrete-filled steel composite columns may be different compared with uniform composite columns. This difference can be because of the existence and change of the tapered angle. The tapered concrete-filled steel composite columns can be a good choice for high and low rise buildings due to their capacity to withstand large loads, have ductile behaviour, and offer architectural advantages. The architectural advantages of these columns can be owing to the infill of concrete which increases the strength of the columns significantly, thus much smaller column sections could be used in this case. The smaller sections of these kinds of the columns result in the considerable saving in usable floor areas in buildings. On the other hand, the lower section of some kinds of the tapered concrete-filled steel composite columns is smaller than the upper one which can make the columns look higher than its real height. Han *et al.* (2010) tested inclined, tapered and straight-tapered-straight concrete-filled steel tubular stub columns. Their tapered columns were square and circular stub columns under axial loading in which the section areas were reduced gradually from the bottom to the top due to the tapered angle. The main parameters of their tapered columns were tapered angle (from the bottom to the top) and cross-sectional type (circular and square). The length of their stub columns was 600 mm. It was concluded that the stub tapered columns behaved in a ductile manner and the cross-sectional strength decreased significantly by the increase of the tapered angle from the bottom to the top. Straight, inclined and tapered stainless steel-concrete-carbon steel double-skin tubular stub columns were experimentally investigated by Han *et al.* (2011). The main variables of their tapered columns were the sectional type (circular, square, round-end rectangular and elliptical) and the hollow ratio of the composite section (from 0.5 to 0.75). Their stub tapered columns were double skin with the lengths of 660 mm and 720 mm which were subjected to axial loading. The tapered angle of the columns tested by Han *et al.* (2011) was the same as that of the tapered columns studied by Han *et al.* (2010). In other words, the tapered angle increased from the bottom to the top of the columns so that the section areas were decreased gradually from the bottom to the top. It was concluded that the tested stub stainless steel-concrete-carbon steel double-skin tubular (DST) columns had good ductility and the cross-sectional strength of the tapered DST columns decreased by the increase of the tapered angle.

Slender rectangular tapered concrete-filled steel composite (TCFSC) columns that are studied in this paper are those kinds of the tapered columns in which the tapered angle increases from their top and bottom to their mid-height. However, study on the structural behaviour of these TCFSC columns has not been widely performed yet.

This paper presents a study on the structural behaviour of tapered concrete-filled steel composite (TCFSC) columns under eccentric loading. In order to verify the finite element modelling, comparison of the result is conducted with the corresponding experimental test result reported by Liu (2006). Nonlinear analyses are performed to study the structural behaviour of the columns under different parameters such as: (1) tapered angle (from 0^o to 2.75^o); (2) steel wall thickness (from 3 mm to 4 mm); (3) load eccentricity (15 mm and 30 mm); (4) L/H ratio (from 10.67 to 17.33); (5) concrete compressive strength (from 30 MPa to 60 MPa); (6) steel yield stress (from 250 MPa to 495 MPa). Effects of change in the tapered angle, steel wall thickness and L/H ratio on the ultimate load capacity, ductility, stiffness, and behaviour of the columns are also presented. In addition, effects of changing the load eccentricity, concrete compressive strength and steel yield stress on the ultimate load capacity and behaviour of the columns are examined.

2. Nonlinear finite element analysis

LUSAS software Version 14 was used to conduct nonlinear finite element analyses herein. LUSAS is one of the world's leading structural analysis systems. By choosing to use LUSAS one joins a large worldwide community of engineers who use LUSAS everyday to solve a wide range of engineering analysis problems. The LUSAS system uses finite element analysis techniques to provide accurate solutions for all types of linear and nonlinear stress, dynamic and thermal/field problems. The two main components of the system are: LUSAS Modeller which is a fully interactive graphical user interface for modelling and viewing of results from an analysis; LUSAS Solver that is a powerful finite element analysis engine which carries out the analysis of the problem defined in LUSAS Modeller (LUSAS 2006).

2.1 Finite element modelling

A concrete-filled steel composite (CFSC) column with the length of 2.6 m and steel wall thickness of 4 mm which experimentally tested by Liu (2006) has been modelled in this paper for the verification of the finite element modelling. Fig. 1 illustrates cross-section of the column herein.

In preparing the CFSC column in the experimental test of Liu (2006), four steel plates were cut and welded along the corners to form a rectangular box in which concrete was poured. Many researches have been conducted on the influence of residual stresses owing to the fabrication especially welding of the steel sheet on the behaviour of CFSC columns. Tao *et al.* (2009)

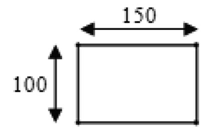

Fig. 1 Cross-section of the CFSC column tested by Liu (2006) (unit: mm)

performed an analysis of CFSC columns without residual stresses and with residual stresses. Their results demonstrated that a slight strength decrease effect was induced. In accordance with them, this effect could be ignored because only a very limited reduction in stiffness and ultimate strength was induced. The strength reduction was generally about 1%. According to Tao *et al.* (2009), although it is believed that the behaviour of thin-walled hollow tubes is often influenced with the residual stresses, this effect is not considerable for a CFSC column, because it is the concrete core of the column which contributes to most of its strength. Also, Uy (1998b) mentioned that fabricated steel box columns are subjected to welding process which causes shrinkage of the weld metal and thereby results in the development of tensile yield stresses at the plate junctions which are equilibrated by residual compressive stresses in the unwelded regions of the box. In order to investigate the effect of residual stresses on the stiffness and strength of a CFSC column, the residual tensile and compressive stresses in the steel box were varied in his study. It was concluded that the effect of residual stresses is such that the initial stiffness of the column is slightly greater until the compressive stresses reach yield and a slight loss of stiffness is encountered because the presence of residual stresses is only effective in the elastic range. According to Uy (1998b), there was no decrease in the ultimate strength induced by residual stresses. This slight effect of residual stresses on the ultimate strength and stiffness of CFSC columns has been also reported by many other researchers such as Furlong (1968), Zhong (1995) and Huang *et al.* (2002).

Although, in accordance with the above-mentioned literature, the residual stresses due to the fabrication process of the steel wall of CFSC columns have a slight effect on the behaviour of the columns, this slight influence has been also considered in the finite element modelling in this study to obtain very accurate results. According to Tao *et al.* (2009), research on residual stresses done by Uy (1998a) has demonstrated that the maximum tensile residual stress occurs near the weld centreline and is typically near or at the yield strength f_y. Test results have also illustrated that the residual stress in compression is about 15-25% of f_y. For simplicity consideration, the residual stress in compression was considered as $0.2f_y$ in finite element modelling by Han (2007) for welded rectangular tubes. This assumption was also adopted by Tao *et al.* (2009) in their finite element modelling of the columns. In this study, the above-mentioned assumption of Han (2007) and Tao *et al.* (2009) has been also adopted in the finite element modelling to consider the effect of residual stresses on the behaviour of the columns.

Type of element for the steel wall and concrete core of the columns was selected from the element library of the LUSAS software (LUSAS 2006) in this study. 6-noded triangular shell element, TSL6, was used for modelling of the steel wall. The element is a thin, doubly curved and isoparametric element which can be utilised to model three-dimensional structures. It provides accurate solution to most applications. This element can accommodate generally curved geometry with varying thickness and anisotropic and composite material properties. The element formulation takes account of both membrane and flexural deformations. 10-noded tetrahedral element, TH10, was used to model the concrete core. This element is a three-dimensional isoparametric solid continuum element capable of modelling curved boundaries. The element is

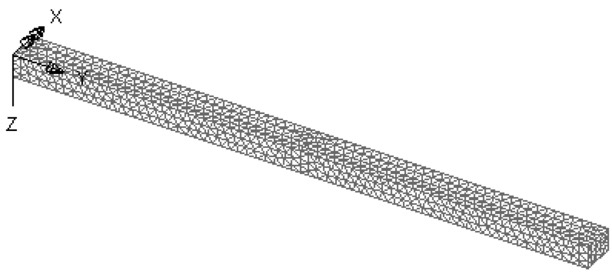

Fig. 2 Typical finite element mesh of the CFSC column

numerically integrated. This type of element is a standard volume element of the LUSAS software (LUSAS 2006). These elements, TSL6 and TH10, can be utilised for linear and complex nonlinear analyses which involve contact, plasticity and large deformations. Small transverse forces were used to create an initial geometric imperfection. Support conditions were appropriately modelled by restraining the nodes corresponding to the support points. The applied eccentric load about the major axis in the experimental test was exactly simulated in the finite element modelling by the use of the displacement control in the negative Y direction acting eccentrically to the column. Different mesh sizes were examined to find a suitable finite element mesh size for the modelling to achieve accurate results. Finally, nonlinear finite element analysis based on the mesh size corresponding to 7538 elements was found to be able to obtain exact results.

A typical finite element mesh of the CFSC column used in this study is shown in Fig. 2.

2.2 Material constitutive models

Material modelling of steel and concrete is an essential part in the constitution of numerical modelling which is explained in the following sections. Material properties adopted by Liu (2006) in the experimental test have been also considered for the modelling verification herein.

2.2.1 Steel

In general, the behaviour of steel between zero and yield stress states is linear elastic and then it behaves plastically, whether it is in compression or tension. Conclusively, a material model which possesses a combination of linear elastic and plastic behaviour is utilised to model the behaviour of steel.

In this study, modelling of steel has been performed as an elastic-perfectly plastic material in both tension and compression. Fig. 3 illustrates the stress-strain curve used for steel. The yield stress and modulus of elasticity of steel have been taken as 495 MPa and 206,000 MPa, respectively. Von Mises yield criterion, an associated flow rule, and isotropic hardening have been used in the nonlinear material model.

2.2.2 Concrete

The compressive strength and modulus of elasticity of concrete have been considered as 60 MPa and 39,000 MPa, respectively. The equivalent uniaxial stress-strain curves for both unconfined and confined concrete (Fig. 4) used by Ellobody and Young (2006a, 2006b) have been also utilised in

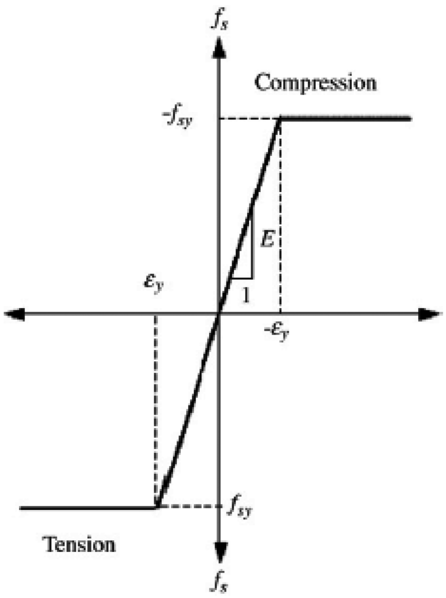

Fig. 3 Stress-strain curve for steel

this study to model concrete. The unconfined concrete cylinder compressive strength f_c is equal to $0.8f_{cu}$, and f_{cu} is the unconfined concrete cube compressive strength. According to Hu *et al.* (2005), the corresponding unconfined strain ε_c is usually around the range of 0.002-0.003. ε_c was taken as 0.002 by Hu *et al.* (2005). The same value for ε_c has been also adopted in the analysis herein. When concrete is under laterally confining pressure, the confined compressive strength f_{cc} and the corresponding confined strain ε_{cc} are much greater than those of unconfined concrete.

Eqs. (1) and (2) proposed by Mander *et al.* (1988) have been used to obtain the confined concrete compressive strength f_{cc} and the corresponding confined stain ε_{cc}:

$$f_{cc} = f_c + k_1 f_1, \tag{1}$$

$$\varepsilon_{cc} = \varepsilon_c\left(1 + k_2\frac{f_1}{f_c}\right) \tag{2}$$

where f_1 is the lateral confining pressure provided by the steel wall. The approximate value of f_1 can be interpolated from the values presented by Hu *et al.* (2003). The factors of k_1 and k_2 have been considered as 4.1 and 20.5, respectively, as reported by Richart *et al.* (1928). Since f_1, k_1 and k_2 are known f_{cc} and ε_{cc} can be obtained by the use of Eqs. (1) and (2). As it is shown in Fig. 4, the equivalent uniaxial stress-strain curve for confined concrete consists of three parts which are needed to be defined. The first part includes the initially assumed elastic range to the proportional limit stress. The value of the proportional limit stress has been chosen as $0.5f_{cc}$ as presented by Hu *et al.* (2003). Also, the initial Young's modulus of confined concrete E_{cc} has been determined using the empirical Eq. (3). The Poisson's ratio υ_{cc} of confined concrete has been adopted as 0.2.

$$E_{cc} = 4700\sqrt{f_{cc}} \text{ MPa} \tag{3}$$

The second part comprises the nonlinear portion which starts from the proportional limit stress

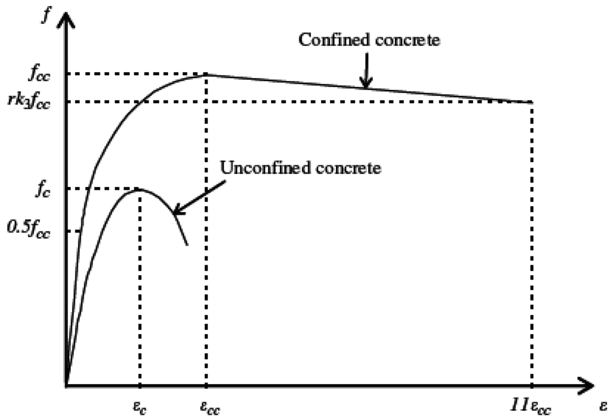

Fig. 4 Equivalent uniaxial stress-strain curves for unconfined and confined concrete

$0.5f_{cc}$ to the confined concrete strength f_{cc}. The common Eq. (4) given by Saenz (1964) can be used to determine this part. The values of uniaxial stress f and strain ε are the unknowns of the equation which define this part of the curve. The strain values ε have been chosen between the proportional strain $(0.5f_{cc}/E_{cc})$, and the confined strain ε_{cc} which corresponds to the confined concrete strength. By assuming the strain values ε, Eq. (4) can be used to determine the stress values f.

$$f = \frac{E_{cc}\varepsilon}{1+(R+R_E-2)\left(\frac{\varepsilon}{\varepsilon_{cc}}\right)-(2R-1)\left(\frac{\varepsilon}{\varepsilon_{cc}}\right)^2+R\left(\frac{\varepsilon}{\varepsilon_{cc}}\right)^3} \tag{4}$$

where

$$R_E = \frac{E_{cc}\varepsilon_{cc}}{f_{cc}}$$

$$R = \frac{R_E(R_\sigma-1)}{(R_\varepsilon-1)^2}-\frac{1}{R_\varepsilon}$$

The constants R_ε and R_σ have been considered as 4 in this study, as recommended by Hu and Schnobrich (1989). The third part of the curve is the descending part which is between f_{cc} and rk_3f_{cc} with the corresponding strain of $11\varepsilon_{cc}$. k_3 is the reduction factor that depends on the H/t ratio and the steel wall yield stress f_y. Empirical equations proposed by Hu *et al.* (2003) can be utilised to calculate the approximate value of k_3. In order to consider the effect of different concrete strengths, the reduction factor r was introduced by Ellobody *et al.* (2006) on the basis of the experimental study performed by Giakoumelis and Lam (2004). In accordance with Tomii (1991) and also Mursi and Uy (2003), the value of r has been considered as 1.0 for concrete with cube strength f_{cu} equal to 30 MPa and as 0.5 for concrete with f_{cu} greater than or equal to 100 MPa. The value of r for concrete cube strength between 30 MPa and 100 MPa has been determined by the use of linear interpolation in this study. A linear Drucker-Prager yield criterion G (Fig. 5) used by Ellobody and Young (2006a, 2006b) and Hu *et al.* (2005) has been also utilised in this paper to model the yielding part of the curve that is the part after the proportional limit stress.

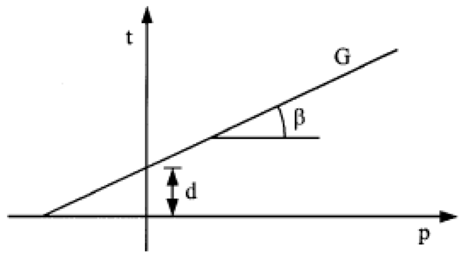

Fig. 5 Linear Drucker-Prager yield criterion for concrete

This criterion has been used to define yield surface and flow potential parameters for concrete under triaxial compressive stresses. Also, this criterion has been utilised with associated flow and isotropic rule and also can be expressed as Eq. (5).

$$G = t - p \tan\beta - d = 0 \tag{5}$$

where t, p and d are determined from the following equations

$$t = \frac{\sqrt{3J_2}}{2}\left(1 + \frac{1}{K} - \left(1 - \frac{1}{K}\right)\left(\frac{r}{\sqrt{3J_2}}\right)^3\right)$$

$$r = \left(\frac{9}{2}(S_1^3 + S_2^3 + S_3^3)\right)^{1/3}$$

$$p = \frac{-(\sigma_1 + \sigma_2 + \sigma_3)}{3}$$

$$d = \left(1 - \frac{\tan\beta}{3}\right)f'_{cc}$$

J_2 is the second stress invariant of the stress deviator tensor, S_1, S_2 and S_3 are the principal stress deviators, and σ_1, σ_2 and σ_3 are the principle stresses. As recommended by Hu *et al.* (2003), the material angle of friction β and the ratio of flow stress in triaxial tension to that in compression K have been considered as 20 and 0.8, respectively.

2.3 Verification of modelling

A comparison was performed between the results of the finite element modelling and the experimental test of Liu (2006) to demonstrate the accuracy of the modelling in this study. According to Fig. 6, the curves lie very close to each other. The ultimate load capacity obtained from the finite element analysis is 1106 kN whilst that from the experiment is 1130 kN. Therefore, the nonlinear finite element analysis underestimates the ultimate load capacity of the column by only 2.1% which shows the accuracy of the modelling. Consequently, the proposed finite element modelling is absolutely capable to predict the structural behaviour of the columns with a very good accuracy herein.

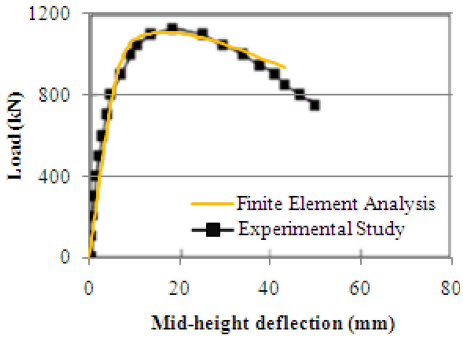

Fig. 6 Load versus mid-height deflection curves for the columns ($L = 2600$ mm, $t = 4$ mm, $\theta = 0°$ and $e = 15$ mm)

3. Numerical analysis

Since it was shown that the proposed finite element modelling of this study is accurate to investigate the structural behaviour of the columns, the method was used for the nonlinear analysis of columns of same cross-section as that tested by Liu (2006) but with various tapered angles, different steel wall thicknesses and several lengths. Each of the tapered concrete-filled steel composite (TCFSC) columns was exactly modelled based on the previously explained modelling specifications. Fig. 7 depicts the geometry of the analysed TCFSC columns using the nonlinear finite element analysis. H_m, B_m and θ indicate the mid-height depth and width, and also the tapered angle of the columns, respectively. According to previous experimental studies which were carried out on the behaviour of slender CFSC columns by other researchers such as Liu (2004, 2006), Tao *et al.* (2007) and Uy *et al.* (2009), the columns failed due to overall buckling with concrete crushing about their mid-height where local buckling of the steel wall occurred. Therefore, it can be concluded that the mid-height of the columns is subjected to higher stresses. Accordingly, if the cross-section in the mid-height of the slender CFSC columns is considered larger than that at the two ends, overall buckling, concrete crushing and local buckling of the columns will be delayed and it is expected to result in higher ultimate load capacity, larger stiffness and better ductility. Because of this reason, the cross-section in the mid-height of the slender CFSC columns has been considered larger than that at the two ends to investigate the behaviour of these kinds of columns in this study. Fig. 8 illustrates a typical finite element mesh of the TCFSC columns. All of the columns were

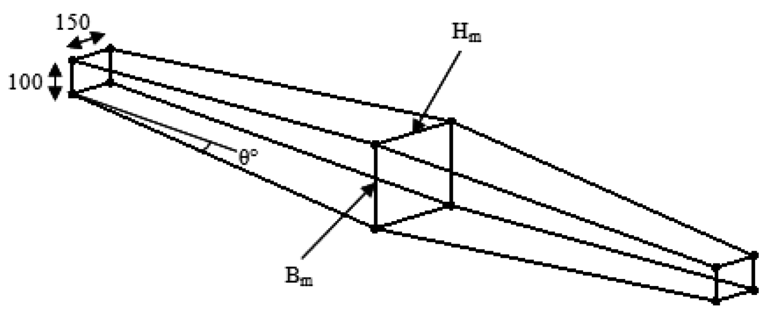

Fig. 7 Geometry of the TCFSC columns ($L = 2600$ mm and $\theta = 0°$-$2.75°$) (unit: mm)

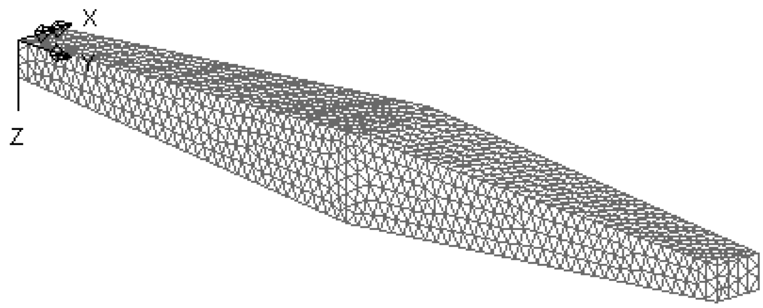

Fig. 8 Typical finite element mesh of the TCFSC columns ($L = 2600$ mm and $\theta = 2.75^o$)

modelled by the use of the LUSAS software. Results obtained from the nonlinear analyses of the columns are presented in the following sections.

4. Results and discussion

Features and ultimate load capacities of the analysed TCFSC columns are provided in Table 1. *C* in the column designations refers to the columns while the following six numbers in the labels are utilised to distinguish the columns with different $H_m \times B_m \times t$ (mm), tapered angles (θ°), L/H ratios, eccentricities (e mm), steel yield stresses f_y (MPa) and concrete compressive strengths f_c (MPa).

Also, the load versus mid-height deflection curves corresponding to the results of Table 1 are presented in the following sections along with effects of different variables on the ultimate load capacity, ductility and stiffness of the TCFSC columns.

4.1 Effect of steel wall thickness on ultimate load capacity

Figs. 9 and 10 illustrate the effect of different steel wall thicknesses ($t = 3$ mm, 3.5 mm and 4 mm) on the ultimate load capacity of the TCFSC columns. The corresponding ultimate load capacity values of the curves are also summarised in Table 1. It can be noticed that change of the steel wall thickness has a significant effect on the ultimate load capacity of the columns. As the steel wall thickness increases, the ultimate load capacity enhances. This point can be due to the fact that a thicker steel wall improves the confinement effect of the steel wall on the concrete core. The improved confinement effect increases the ultimate load capacity. For example, the ultimate load capacity of the column *C*9-2-17-30-495-60 with the steel wall thickness of 3 mm is 953 kN which enhances to 1067 kN by the use of the column *C*7-2-17-30-495-60 with the steel wall thickness of 4 mm, an increase of 12%.

4.2 Effect of tapered angle on ultimate load capacity

The effect of various tapered angles ($\theta = 0^o$, 0.55^o, 1.10^o, 1.65^o, 2.20^o and 2.75^o) on the ultimate load capacity of the TCFSC columns is shown in Fig. 11. According to the figure and Table 1, the ultimate load capacity of the columns is considerably influenced by change of the tapered angle. Increasing the tapered angle from 0^o to 2.75^o improves the ultimate load capacity. It can be due to

Table 1 Features and ultimate load capacities (N_u) of the columns

No.	Column label	$H_m \times B_m \times t$ (mm)	Tapered angle (θ^o)	L (mm)	L/H	e (mm)	f_y (MPa)	f_c (MPa)	N_u (kN)
1	C1-0-17-15-495-60	150×100×4	0	2600	17.33	15	495	60	1106
2	C2-0-17-15-495-60	150×100×3.5	0	2600	17.33	15	495	60	1037
3	C3-0-17-15-495-60	150×100×3	0	2600	17.33	15	495	60	960
4	C4-1-17-15-495-60	175×125×4	0.55	2600	17.33	15	495	60	1149
5	C5-1-17-15-495-60	175×125×3.5	0.55	2600	17.33	15	495	60	1089
6	C6-1-17-15-495-60	175×125×3	0.55	2600	17.33	15	495	60	1024
7	C7-2-17-15-495-60	200×150×4	1.10	2600	17.33	15	495	60	1234
8	C8-2-17-15-495-60	200×150×3.5	1.10	2600	17.33	15	495	60	1185
9	C9-2-17-15-495-60	200×150×3	1.10	2600	17.33	15	495	60	1132
10	C10-3-17-15-495-60	225×175×4	1.65	2600	17.33	15	495	60	1272
11	C11-3-17-15-495-60	225×175×3.5	1.65	2600	17.33	15	495	60	1222
12	C12-3-17-15-495-60	225×175×3	1.65	2600	17.33	15	495	60	1169
13	C13-4-17-15-495-60	250×200×4	2.20	2600	17.33	15	495	60	1306
14	C14-4-17-15-495-60	250×200×3.5	2.20	2600	17.33	15	495	60	1255
15	C15-4-17-15-495-60	250×200×3	2.20	2600	17.33	15	495	60	1202
16	C16-5-17-15-495-60	275×225×4	2.75	2600	17.33	15	495	60	1336
17	C17-5-17-15-495-60	275×225×3.5	2.75	2600	17.33	15	495	60	1286
18	C18-5-17-15-495-60	275×225×3	2.75	2600	17.33	15	495	60	1232
19	C1-0-17-30-495-60	150×100×4	0	2600	17.33	30	495	60	864
20	C2-0-17-30-495-60	150×100×3.5	0	2600	17.33	30	495	60	786
21	C3-0-17-30-495-60	150×100×3	0	2600	17.33	30	495	60	706
22	C4-1-17-30-495-60	175×125×4	0.55	2600	17.33	30	495	60	920
23	C5-1-17-30-495-60	175×125×3.5	0.55	2600	17.33	30	495	60	843
24	C6-1-17-30-495-60	175×125×3	0.55	2600	17.33	30	495	60	768
25	C7-2-17-30-495-60	200×150×4	1.10	2600	17.33	30	495	60	1067
26	C8-2-17-30-495-60	200×150×3.5	1.10	2600	17.33	30	495	60	1013
27	C9-2-17-30-495-60	200×150×3	1.10	2600	17.33	30	495	60	953
28	C10-3-17-30-495-60	225×175×4	1.65	2600	17.33	30	495	60	1139
29	C11-3-17-30-495-60	225×175×3.5	1.65	2600	17.33	30	495	60	1088
30	C12-3-17-30-495-60	225×175×3	1.65	2600	17.33	30	495	60	1032
31	C13-4-17-30-495-60	250×200×4	2.20	2600	17.33	30	495	60	1171
32	C14-4-17-30-495-60	250×200×3.5	2.20	2600	17.33	30	495	60	1122
33	C15-4-17-30-495-60	250×200×3	2.20	2600	17.33	30	495	60	1070
34	C16-5-17-30-495-60	275×225×4	2.75	2600	17.33	30	495	60	1206
35	C17-5-17-30-495-60	275×225×3.5	2.75	2600	17.33	30	495	60	1158
36	C18-5-17-30-495-60	275×225×3	2.75	2600	17.33	30	495	60	1106
37	C1-0-14-15-495-60	150×100×4	0	2100	14	15	495	60	1170
38	C19-1-14-15-495-60	170×120×4	0.55	2100	14	15	495	60	1213
39	C20-2-14-15-495-60	190×140×4	1.10	2100	14	15	495	60	1298
40	C21-3-14-15-495-60	210×160×4	1.65	2100	14	15	495	60	1335
41	C22-4-14-15-495-60	231×181×4	2.20	2100	14	15	495	60	1369

Table 1 Continued

No.	Column label	$H_m \times B_m \times t$ (mm)	Tapered angle (θ^o)	L (mm)	L/H	e (mm)	f_y (MPa)	f_c (MPa)	N_u (kN)
42	*C*23-5-14-15-495-60	251×201×4	2.75	2100	14	15	495	60	1397
43	*C*1-0-10-15-495-60	150×100×4	0	1600	10.67	15	495	60	1251
44	*C*24-1-10-15-495-60	165×115×4	0.55	1600	10.67	15	495	60	1288
45	*C*25-2-10-15-495-60	181×131×4	1.10	1600	10.67	15	495	60	1371
46	*C*26-3-10-15-495-60	196×146×4	1.65	1600	10.67	15	495	60	1404
47	*C*27-4-10-15-495-60	211×161×4	2.20	1600	10.67	15	495	60	1435
48	*C*28-5-10-15-495-60	227×177×4	2.75	1600	10.67	15	495	60	1462
49	*C*13-4-17-15-495-50	250×200×4	2.20	2600	17.33	15	495	50	1172
50	*C*13-4-17-15-495-40	250×200×4	2.20	2600	17.33	15	495	40	1031
51	*C*13-4-17-15-495-30	250×200×4	2.20	2600	17.33	15	495	30	881
52	*C*16-5-17-15-495-50	275×225×4	2.75	2600	17.33	15	495	50	1199
53	*C*16-5-17-15-495-40	275×225×4	2.75	2600	17.33	15	495	40	1055
54	*C*16-5-17-15-495-30	275×225×4	2.75	2600	17.33	15	495	30	902
55	*C*13-4-17-30-495-50	250×200×4	2.20	2600	17.33	30	495	50	1051
56	*C*13-4-17-30-495-40	250×200×4	2.20	2600	17.33	30	495	40	924
57	*C*13-4-17-30-495-30	250×200×4	2.20	2600	17.33	30	495	30	791
58	*C*16-5-17-30-495-50	275×225×4	2.75	2600	17.33	30	495	50	1080
59	*C*16-5-17-30-495-40	275×225×4	2.75	2600	17.33	30	495	40	949
60	*C*16-5-17-30-495-30	275×225×4	2.75	2600	17.33	30	495	30	809
61	*C*13-4-17-15-350-60	250×200×4	2.20	2600	17.33	15	350	60	1145
62	*C*13-4-17-15-250-60	250×200×4	2.20	2600	17.33	15	250	60	1019
63	*C*16-5-17-15-350-60	275×225×4	2.75	2600	17.33	15	350	60	1173
64	*C*16-5-17-15-250-60	275×225×4	2.75	2600	17.33	15	250	60	1045
65	*C*13-4-17-30-350-60	250×200×4	2.20	2600	17.33	30	350	60	1026
66	*C*13-4-17-30-250-60	250×200×4	2.20	2600	17.33	30	250	60	912
67	*C*16-5-17-30-350-60	275×225×4	2.75	2600	17.33	30	350	60	1059
68	*C*16-5-17-30-250-60	275×225×4	2.75	2600	17.33	30	250	60	943

the point that the enhancement of the tapered angle of the slender columns improves their strength at the mid-height which delays their overall buckling and results in higher ultimate load capacity. For instance, by the enhancement of the tapered angle from 0^o (*C*3-0-17-15-495-60) to 2.75^o (*C*18-5-17-15-495-60) the ultimate load capacity increases from 960 kN to 1232 kN, an enhancement of 28.3%.

4.3 Effect of load eccentricity on ultimate load capacity

Fig. 12 indicates the effect of the load eccentricities (15 mm and 30 mm) on the ultimate load capacity of the columns. As it is obvious from the figure, the ultimate load capacity of the columns is adversely affected by the load eccentricity. For example, increasing the load eccentricity from 15 mm (*C*5-1-17-15-495-60) to 30 mm (*C*5-1-17-30-495-60) reduces the ultimate load capacity from 1089 kN to 843 kN, a reduction of 22.6%. Similar trends can be observed for the ultimate load

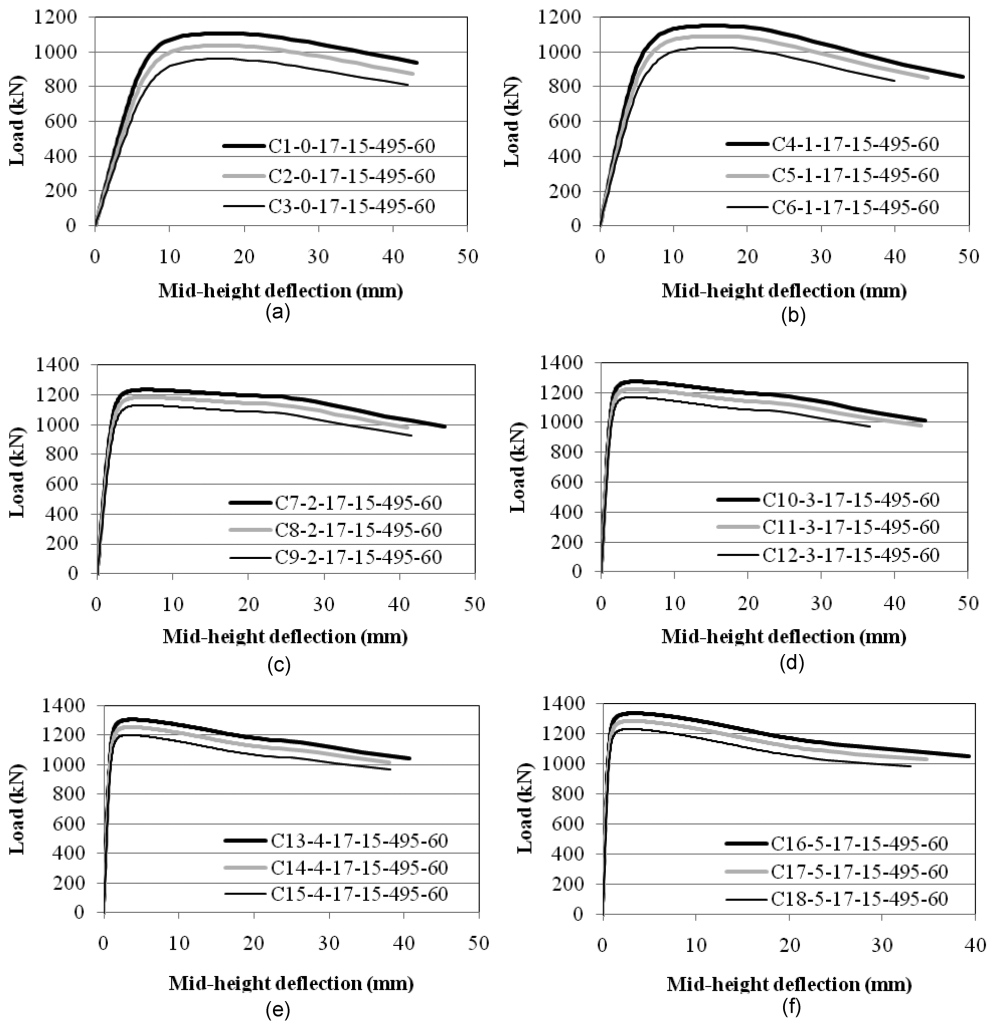

Fig. 9 Load versus mid-height deflection curves for the columns (e = 15 mm): (a) $\theta = 0°$, (b) $\theta = 0.55°$, (c) $\theta = 1.10°$, (d) $\theta = 1.65°$, (e) $\theta = 2.20°$ and (f) $\theta = 2.75°$

capacity of the columns with other concrete compressive strengths (30 MPa, 40 MPa and 50 MPa) and steel yield stresses (250 MPa and 350 MPa) in Table 1.

Also, the decrease percentages of the ultimate load capacity are summarised in Table 2 based on the increase of the load eccentricity from 15 mm to 30 mm. According to the table, as the tapered angle is enhanced (from 0^{o} to 2.75^{o}) for the same steel wall thickness, the decrease percentage of the ultimate load capacity is reduced in a descending order. This issue can be because of the point that by the increase of the load eccentricity the columns might tend to deflect more at their mid-height. On the other hand, as the tapered angle of the columns is increased the strength of their mid-height is enhanced which results in the decrease of the deflection at their mid-height. This decrease of the mid-height deflection increases the ultimate load capacity, i.e., reduces the decrease percentage of the ultimate load capacity.

Moreover, it can be noticed from Table 2 that as the steel wall thickness of the columns is

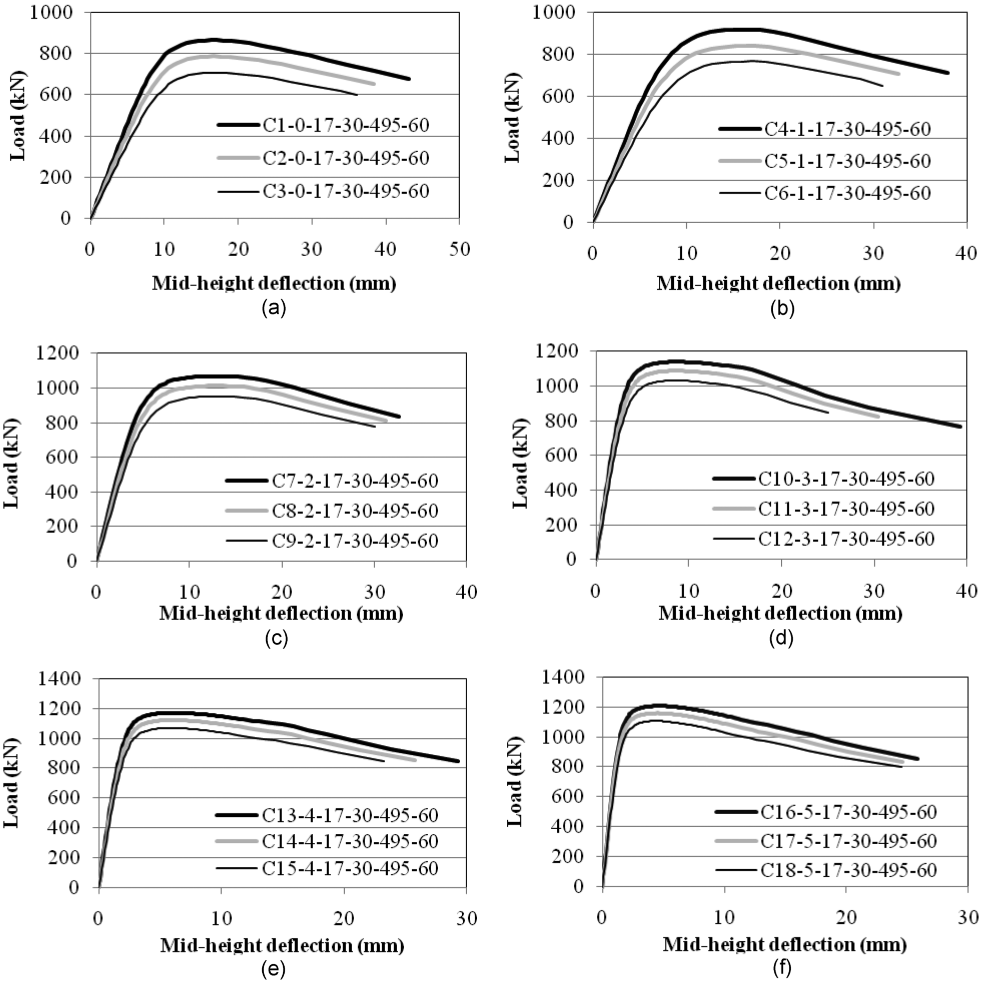

Fig. 10 Load versus mid-height deflection curves for the columns ($e = 30$ mm): (a) $\theta = 0°$, (b) $\theta = 0.55°$, (c) $\theta = 1.10°$, (d) $\theta = 1.65°$, (e) $\theta = 2.20°$ and (f) $\theta = 2.75°$

increased (from 3 mm to 4 mm) for the same tapered angle, the decrease percentage of the ultimate load capacity is reduced in a descending order. Because, as the steel wall thickness is enhanced more confinement effect is provided for the concrete core by the steel wall. The improved confinement effect leads to higher ultimate load capacity, i.e., results in the reduction of the decrease percentage of the ultimate load capacity.

4.4 Effects of tapered angle and steel wall thickness on ductility

Effects of the tapered angle and steel wall thickness on the ductility of the columns are investigated in this study by the use of a ductility index defined by Tao and Han (2007):

$$DI = \frac{u_{85\%}}{u_y} \tag{6}$$

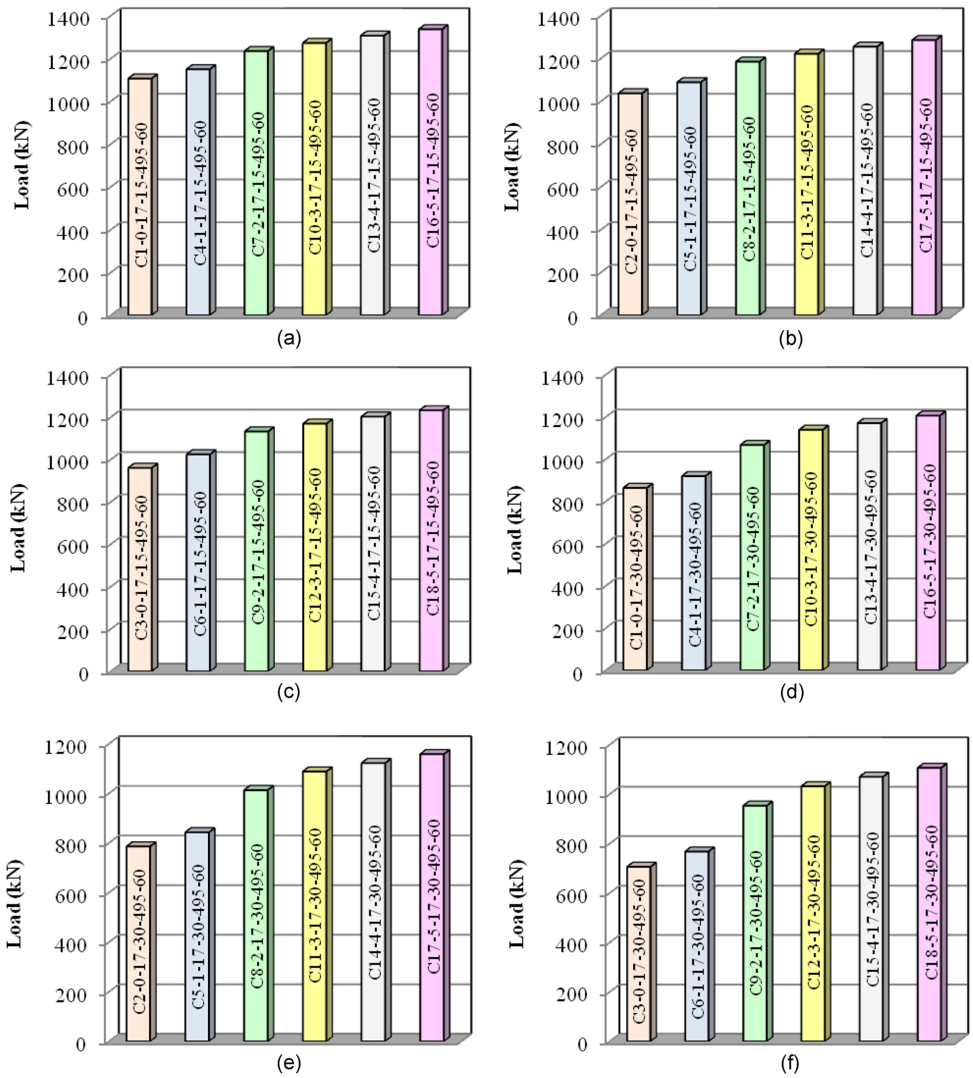

Fig. 11 Effect of tapered angle (θ = 0°-2.75°) on the ultimate load capacity: (a) e = 15 mm, t = 4 mm, (b) e = 15 mm, t = 3.5 mm, (c) e = 15 mm, t = 3 mm, (d) e = 30 mm, t = 4 mm, (e) e = 30 mm, t = 3.5 mm and (f) e = 30 mm, t = 3 mm

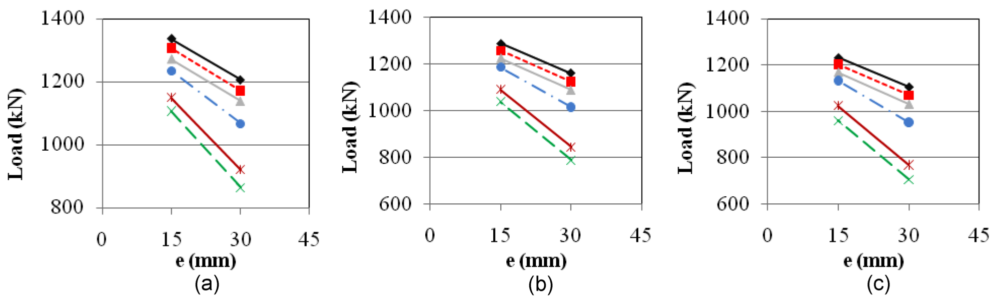

Fig. 12 Effect of load eccentricity on the ultimate load capacity (θ = 0°-2.75°, f_c = 60 MPa and f_y = 495 MPa): (a) t = 4 mm, (b) t = 3.5 mm and (c) t = 3 mm

Table 2 Decrease percentage of the ultimate load capacity based on the increase of load eccentricity from 15 to 30 mm (f_c = 60 MPa and f_y = 495 MPa)

	Decrease percentage of the ultimate load capacity					
Steel wall thickness, t (mm)	θ = 0°	θ = 0.55°	θ = 1.10°	θ = 1.65°	θ = 2.20°	θ = 2.75°
4	21.9%	19.9%	13.5%	10.5%	10.3%	9.7%
3.5	24.2%	22.6%	14.5%	11%	10.6%	10%
3	26.5%	25%	15.8%	11.7%	11%	10.2%

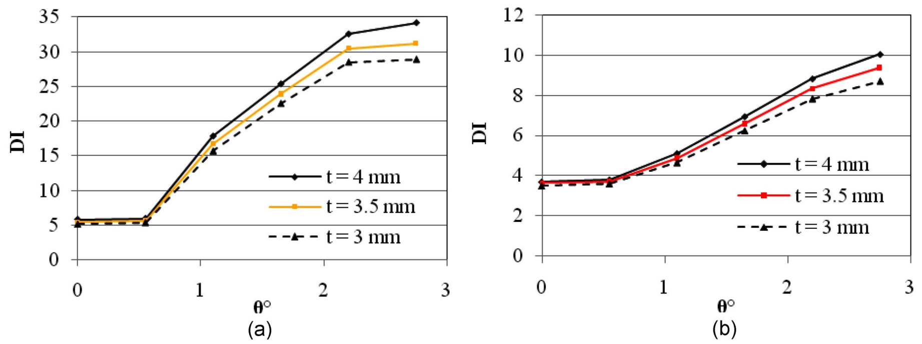

Fig. 13 Effect of tapered angle and steel wall thickness on the ductility (θ= 0°-2.75°, f_c = 60 MPa and f_y = 495 MPa): (a) e = 15 mm and (b) e = 30 mm

where $u_{85\%}$ is the mid-height deflection of the columns corresponding to the load which drops to 85% of the ultimate load capacity and u_y is $u_{75\%}/0.75$ in which $u_{75\%}$ is the mid-height deflection of the columns corresponding to the load that obtains 75% of the ultimate load capacity. The values of $u_{85\%}$ and u_y can be taken from Figs. 9 and 10. Effects of the tapered angle and steel wall thickness on the ductility are illustrated in Fig. 13. As can be seen from this figure, change of the tapered angle is noticeably effective on the ductility of the columns. According to the figure, by the increase of the tapered angle from 0° to 2.75°, the ductility of the columns is enhanced. The figure shows that the gradient of the lines is low for change of the tapered angle from 0° to 0.55° but it gets considerably higher as the angle is increased from 0.55° to 2.75°. This point uncovers the effectiveness of the enhancement of the tapered angle from 0.55° to 2.75° on the improvement of the ductility compared with that from 0° to 0.55°. For example, the ductility of the column *C*2-0-17-30-495-60 (θ = 0°) is 3.643 which increases to 3.724, 4.881, 6.588, 8.329 and 9.371 respectively for the columns *C*5-1-17-30-495-60 (θ= 0.55°), *C*8-2-17-30-495-60 (θ= 1.10°), *C*11-3-17-30-495-60 (θ= 1.65°), *C*14-4-17-30-495-60 (θ= 2.20°) and *C*17-5-17-30-495-60 (θ= 2.75°).

Also, the effect of the steel wall thickness on the ductility can be observed from Fig. 13. In accordance with the figure, change of the steel wall thickness has a significant effect on the ductility. Increasing the steel wall thickness from 3 mm to 4 mm improves the ductility of the columns. For instance, increasing the steel wall thickness from 3 mm (*C*15-4-17-15-495-60) to 4 mm (*C*13-4-17-15-495-60) enhances the ductility from 28.448 to 32.573, an enhancement of 14.5%.

In addition, when the load obtains its ultimate (Figs. 9 and 10) it decreases slowly which demonstrates the favourable ductility in the post-yield behaviour of the columns.

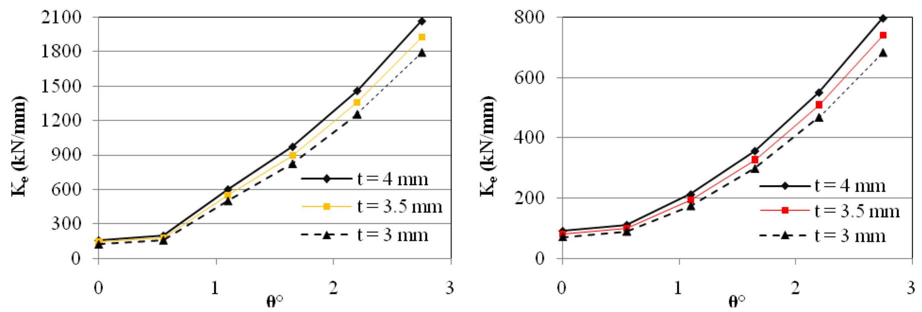

Fig. 14 Effect of tapered angle and steel wall thickness on the stiffness (θ= 0°-2.75°): (a) e = 15 mm and (b) e = 30 mm

4.5 Effects of tapered angle and steel wall thickness on stiffness

To examine effects of the tapered angle and steel wall thickness on the stiffness of the columns, load versus mid-height deflection curves illustrated in Figs. 9 and 10 are used. The stiffness K_e defined by Tao and Han (2007) as secant modulus corresponding to 0.6 of the ultimate load capacity in the pre-peak stage is used herein. Fig. 14 shows theses effects on the stiffness of the columns. According to the figure, changing the tapered angle is remarkably effective on the stiffness. The higher tapered angle leads to the higher stiffness. As can be seen from the figure, the gradient of the lines is low for change of the tapered angle from 0^o to 0.55^o but it gets remarkably higher as the angle is enhanced from 0.55^o to 2.75^o. This issue reveals the effectiveness of increasing the tapered angle from 0.55^o to 2.75^o on the stiffness in comparison with that from 0^o to 0.55^o. Also, it can be noticed from the figure that change of the steel wall thickness noticeably influences the stiffness of the columns. As the steel wall thickness increases from 3 mm to 4 mm the stiffness is improved. The enhancement of the stiffness by increasing the tapered angle and steel wall thickness of the columns can be attributed to the improvement of the confinement effect of the steel wall on the concrete core.

4.6 Effect of concrete compressive strength on ultimate load capacity

Fig. 15 and Table 1 indicate the effect of different concrete compressive strengths (30 MPa, 40 MPa, 50 MPa and 60 MPa) on the ultimate load capacity of the columns. Load axis of each group of curves (a, b, c and d) in Fig. 15 has been normalised based on the ultimate load capacity of the column with the concrete compressive strength of 30 MPa of that group. It is obvious from the figure and the table that change of the concrete compressive strength significantly affects the ultimate load capacity of the columns. Enhancing the concrete compressive strength improves the ultimate load capacity of the columns. For instance, the increase of the concrete compressive strength from 30 MPa (C13-4-17-15-495-30) to 60 MPa (C13-4-17-15-495-60) improves the ultimate load capacity from 881 kN to 1306 kN, an enhancement of 48.2%.

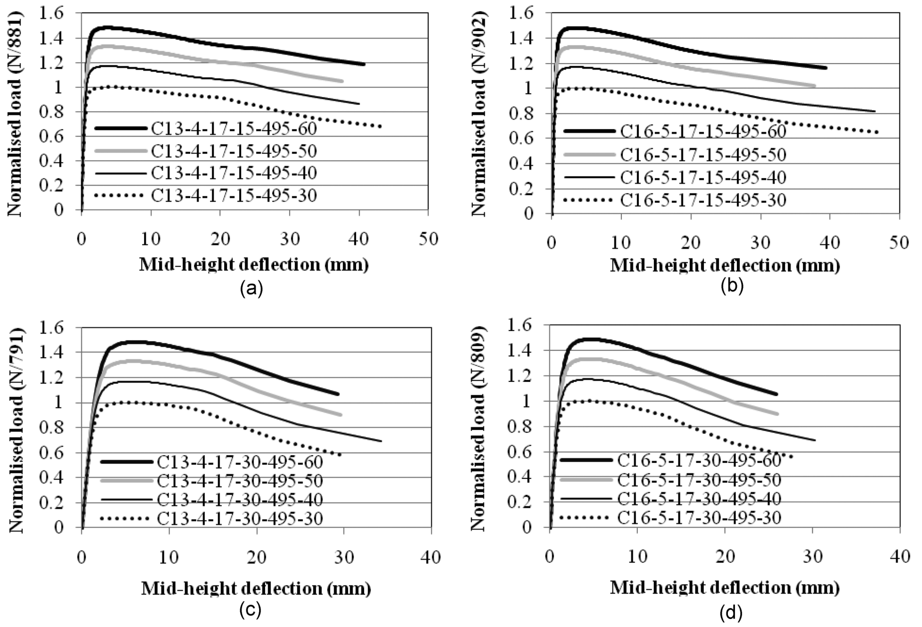

Fig. 15 Effect of concrete compressive strength on the ultimate load capacity ($t = 4$ mm): (a) $\theta = 2.20°$, $e = 15$ mm, (b) $\theta = 2.75°$, $e = 15$ mm, (c) $\theta = 2.20°$, $e = 30$ mm and (d) $\theta = 2.75°$, $e = 30$ mm

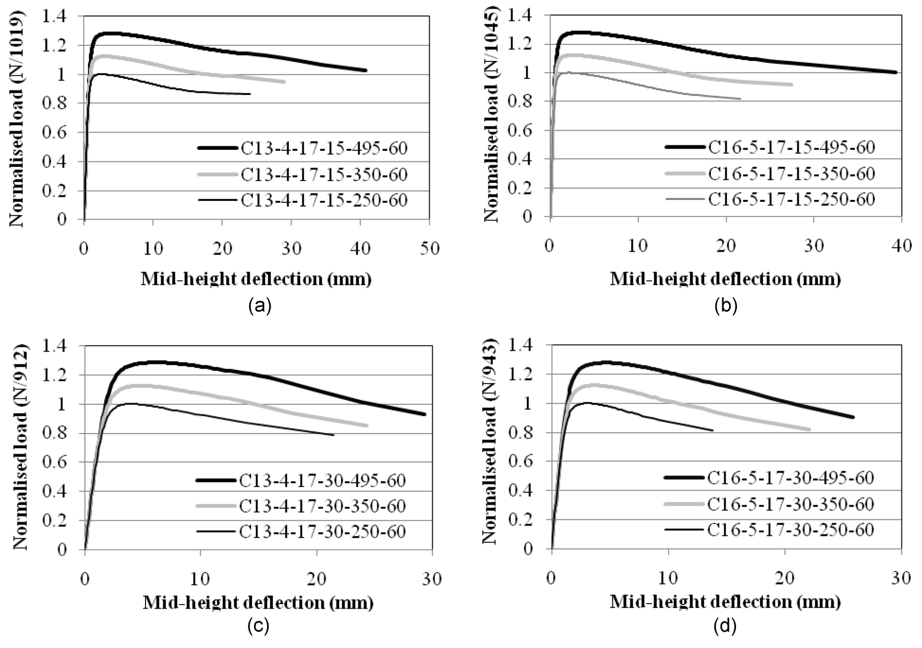

Fig. 16 Effect of steel yield stress on the ultimate load capacity ($t = 4$ mm): (a) $\theta = 2.20°$, $e = 15$ mm, (b) $\theta = 2.75°$, $e = 15$ mm, (c) $\theta = 2.20°$, $e = 30$ mm and (d) $\theta = 2.75°$, $e = 30$ mm

4.7 Effect of steel yield stress on ultimate load capacity

Effect of different steel yield stresses (250 MPa, 350 MPa and 495 MPa) on the ultimate load capacity of the columns is illustrated in Fig. 16 and Table 1. Load axis of each group of curves (a, b, c and d) in Fig. 16 has been normalised on the basis of the ultimate load capacity of the column with the steel yield stress of 250 MPa of that group. In accordance with the figure and the table, the ultimate load capacity of the columns is remarkably affected by change of the steel yield stress. As the steel yield stress is enhanced the ultimate load capacity is improved. For example, as the steel yield stress increases from 250 MPa (*C*16-5-17-30-250-60) to 495 MPa (*C*16-5-17-30-495-60) the ultimate load capacity enhances from 943 MPa to 1206 MPa, an improvement of 27.9%.

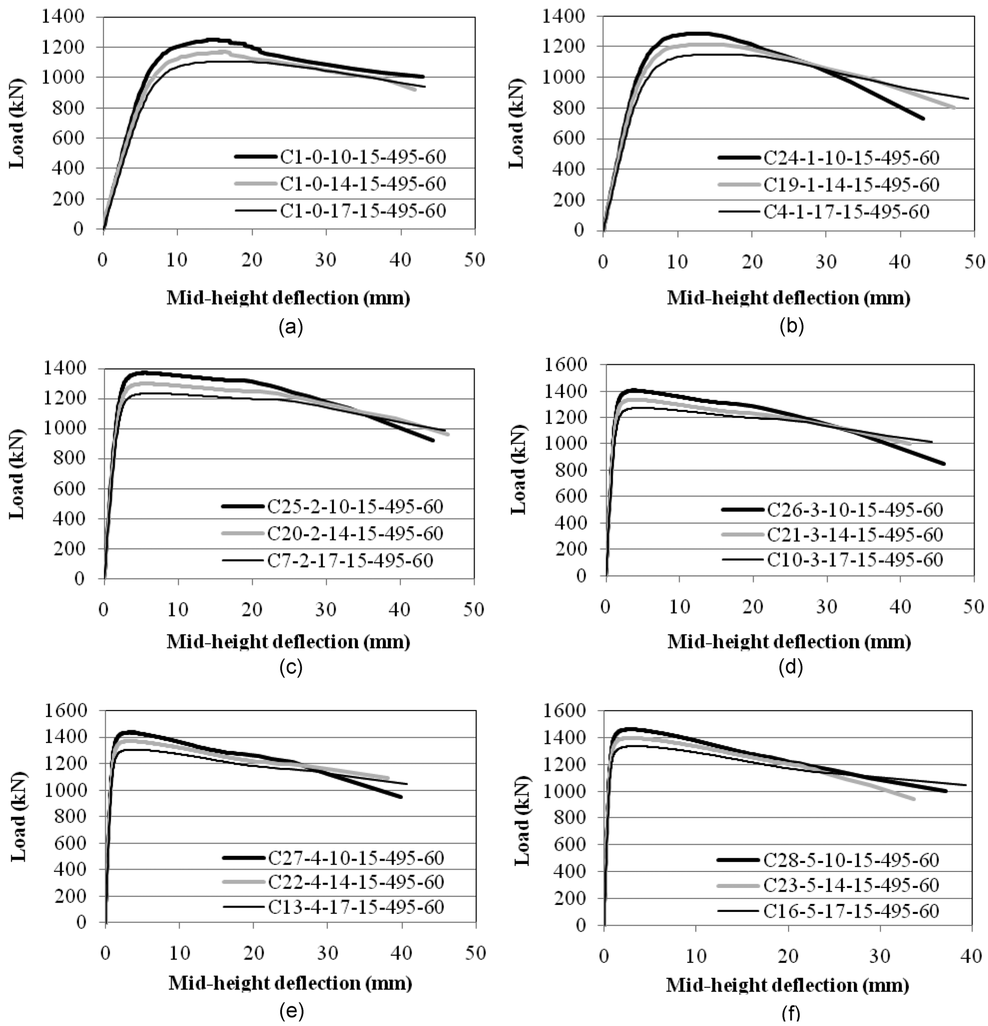

Fig. 17 Effect of L/H ratio on the ultimate load capacity ($e = 15$ mm and $t = 4$ mm): (a) $\theta = 0°$, (b) $\theta = 0.55°$, (c) $\theta = 1.10°$, (d) $\theta = 1.65°$, (e) $\theta = 2.20°$ and (f) $\theta = 2.75°$

4.8 Effect of L/H ratio on ultimate load capacity

Different *L*/*H* ratios of 10.67, 14 and 17.33 which respectively correspond to the column lengths of 1600 mm, 2100 mm and 2600 mm are considered to investigate the effect of the *L*/*H* ratios on the behaviour of the columns. Fig. 17 illustrates the effect of the *L*/*H* ratios (10.67, 14 and 17.33) on the ultimate load capacity of the TCFSC columns and Table 1 tabulates its corresponding values. As can be seen from the figure and table, the ultimate load capacity of the columns is increased by the decrease of the *L*/*H* ratio. For example, the ultimate load capacity of the column *C*4-1-17-15-495-60 with the *L*/*H* ratio of 17.33 is 1149 kN which is increased to 1288 kN by using the column *C*24-1-10-15-495-60 with the *L*/*H* ratio of 10.67, an increase of 12.1%.

On the other hand, as the *L*/*H* ratio increases, the effect of increasing the tapered angle on the enhancement of the ultimate load capacity is enhanced. For instance, as the tapered angle is increased from 0° to 2.75° for the columns with the *L*/*H* ratio of 10.67, the ultimate load capacity is enhanced from 1251 kN (*C*1-0-10-15-495-60) to 1462 kN (*C*28-5-10-15-495-60), an increase of 16.9%. Whilst, the ultimate load capacity is enhanced from 1106 kN (*C*1-0-17-15-495-60) to 1336 kN (*C*16-5-17-15-495-60) for the same increase of the tapered angle for the columns with the *L*/*H* ratio of 17.33, an enhancement of 20.8%.

4.9 Effect of L/H ratio on ductility

Eq. (6) of the section 4.4 is used to determine the ductility of the columns with different *L*/*H* ratios. The values of $u_{85\%}$ and u_y in Eq. (6) can be taken from Fig. 17. Fig. 18 illustrates the effect of the *L*/*H* ratios (10.67, 14 and 17.33) on the ductility. According to the figure, the increase of the *L*/*H* ratio enhances the ductility of the columns. As an example, if the *L*/*H* ratio increases from 10.67 (*C*24-1-10-15-495-60) to 17.33 (*C*4-1-17-15-495-60), the ductility enhances from 4.821 to 5.982, an increase of 24.1%.

In addition, it is obvious from the figure that as the tapered angle is enhanced the ductility of the columns is improved for all the *L*/*H* ratios of 10.67, 14 and 17.33.

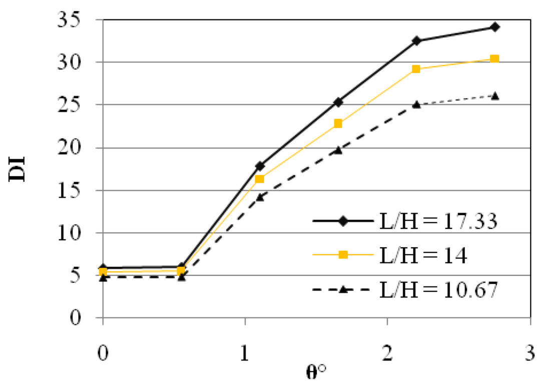

Fig. 18 Effect of *L*/*H* ratio on the ductility (θ= 0°-2.75°, t = 4 mm and e = 15 mm)

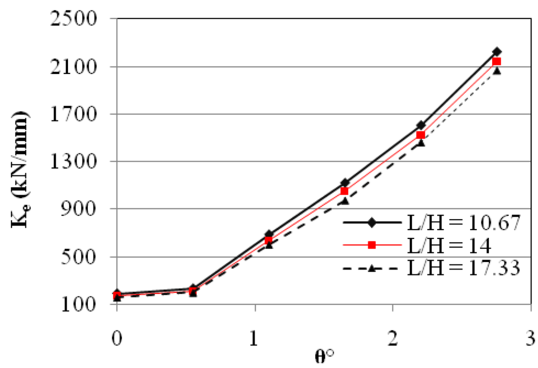

Fig. 19 Effect of *L*/*H* ratio on the stiffness (θ= 0°-2.75°, t = 4 mm and e = 15 mm)

4.10 Effect of L/H ratio on stiffness

The process of obtaining stiffness explained in the section 4.5 is followed to determine the stiffness of the columns with different L/H ratios. The effect of the L/H ratios (10.67, 14 and 17.33) on the stiffness is shown in Fig. 19. In accordance with the figure, the stiffness of the columns is increased by the decrease of the L/H ratio.

Moreover, the increase of the tapered angle enhances the stiffness of the columns for all the L/H ratios of 10.67, 14 and 17.33 (Fig. 19).

Table 3 Comparison of increased A_s and V_c with increased ultimate load capacity

No.	Column label	A_s (mm^2)	V_c (mm^3)	ΔA_s*	ΔV_c*	N_u (kN)	ΔN_u*
1	C1-0-17-15-495-60	1216800	33966400	0.000	0.000	1106	0.000
2	C2-0-17-15-495-60	1227200	34577400	0.000	0.000	1037	0.000
3	C3-0-17-15-495-60	1237600	35193600	0.000	0.000	960	0.000
4	C4-1-17-15-495-60	1346800	42383900	0.107	0.248	1149	0.039
5	C5-1-17-15-495-60	1357200	43059900	0.106	0.245	1089	0.050
6	C6-1-17-15-495-60	1367600	43741100	0.105	0.243	1024	0.067
7	C7-2-17-15-495-60	1476800	52426400	0.214	0.543	1234	0.116
8	C8-2-17-15-495-60	1487200	53167400	0.212	0.538	1185	0.143
9	C9-2-17-15-495-60	1497600	53913600	0.210	0.532	1132	0.179
10	C10-3-17-15-495-60	1606800	64093900	0.321	0.887	1272	0.150
11	C11-3-17-15-495-60	1617200	64899900	0.318	0.877	1222	0.178
12	C12-3-17-15-495-60	1627600	65711100	0.315	0.867	1169	0.218
13	C13-4-17-15-495-60	1736800	77386400	0.427	1.278	1306	0.181
14	C14-4-17-15-495-60	1747200	78257400	0.424	1.263	1255	0.210
15	C15-4-17-15-495-60	1757600	79133600	0.420	1.249	1202	0.252
16	C16-5-17-15-495-60	1866800	92303900	0.534	1.718	1336	0.208
17	C17-5-17-15-495-60	1877200	93239900	0.530	1.697	1286	0.240
18	C18-5-17-15-495-60	1887600	94181100	0.525	1.676	1232	0.283
19	C1-0-17-30-495-60	1216800	33966400	0.000	0.000	864	0.000
20	C2-0-17-30-495-60	1227200	34577400	0.000	0.000	786	0.000
21	C3-0-17-30-495-60	1237600	35193600	0.000	0.000	706	0.000
22	C4-1-17-30-495-60	1346800	42383900	0.107	0.248	920	0.065
23	C5-1-17-30-495-60	1357200	43059900	0.106	0.245	843	0.073
24	C6-1-17-30-495-60	1367600	43741100	0.105	0.243	768	0.088
25	C7-2-17-30-495-60	1476800	52426400	0.214	0.543	1067	0.235
26	C8-2-17-30-495-60	1487200	53167400	0.212	0.538	1013	0.289
27	C9-2-17-30-495-60	1497600	53913600	0.210	0.532	953	0.350
28	C10-3-17-30-495-60	1606800	64093900	0.321	0.887	1139	0.318
29	C11-3-17-30-495-60	1617200	64899900	0.318	0.877	1088	0.384
30	C12-3-17-30-495-60	1627600	65711100	0.315	0.867	1032	0.462
31	C13-4-17-30-495-60	1736800	77386400	0.427	1.278	1171	0.355

Table 3 Continued

No.	Column label	A_s (mm^2)	V_c (mm^3)	ΔA_s*	ΔV_c*	N_u (kN)	ΔN_u*
32	C14-4-17-30-495-60	1747200	78257400	0.424	1.263	1122	0.427
33	C15-4-17-30-495-60	1757600	79133600	0.420	1.249	1070	0.516
34	C16-5-17-30-495-60	1866800	92303900	0.534	1.718	1206	0.396
35	C17-5-17-30-495-60	1877200	93239900	0.530	1.697	1158	0.473
36	C18-5-17-30-495-60	1887600	94181100	0.525	1.676	1106	0.567
37	C1-0-14-15-495-60	982800	27434400	0.000	0.000	1170	0.000
38	C19-1-14-15-495-60	1066800	32768400	0.085	0.194	1213	0.037
39	C20-2-14-15-495-60	1150800	38942400	0.171	0.419	1298	0.109
40	C21-3-14-15-495-60	1234800	45956400	0.256	0.675	1335	0.141
41	C22-4-14-15-495-60	1323000	54225150	0.346	0.977	1369	0.170
42	C23-5-14-15-495-60	1407000	62961150	0.432	1.295	1397	0.194
43	C1-0-10-15-495-60	748800	20902400	0.000	0.000	1251	0.000
44	C24-1-10-15-495-60	796800	23890400	0.064	0.143	1288	0.030
45	C25-2-10-15-495-60	848000	27474400	0.132	0.314	1371	0.096
46	C26-3-10-15-495-60	896000	31206400	0.197	0.493	1404	0.122
47	C27-4-10-15-495-60	944000	35298400	0.261	0.689	1435	0.147
48	C28-5-10-15-495-60	995200	40060000	0.329	0.917	1462	0.169

*Note: Values of ΔA_s, ΔV_c and ΔN_u for all columns have been respectively determined based on the values of A_s, V_c and N_u of their corresponding columns with $\theta = 0°$.

4.11 Comparison of increased A_s and V_c with increased ultimate load capacity

Table 3 summarises the total area of the steel wall, A_s (mm^2), total volume of the concrete core, V_c (mm^3) and the ultimate load capacity, N_u, along with their enhanced values due to the increase of the tapered angle respectively as ΔA_s, ΔV_c and ΔN_u. Based on ΔA_s, ΔV_c and ΔN_u, the effectiveness of these kinds of the columns is completely obvious from the ultimate load capacity view. As can be seen from the table, ΔA_s and ΔV_c are enhanced by each angle increase and the improvement of ΔN_u up to the second angle increase (1.10) is higher than those in the other angle increases (1.10°-2.75°). This point can be resulted in the selection of an optimised angle. For example, the values of ΔN_u for C6-1-17-30-495-60 (θ= 0.55°), C9-2-17-30-495-60 (θ= 1.10°), C12-3-17-30-495-60 (θ= 1.65°), C15-4-17-30-495-60 (θ= 2.20°) and C18-5-17-30-495-60 (θ= 2.75°) are respectively as 8.8%, 35%, 46.2%, 51.6% and 56.7%. Therefore, differences in the above-mentioned values of ΔN_u in each angle increase of 0° to 0.55°, 0.55° to 1.10°, 1.10° to 1.65°, 1.65° to 2.20° and 2.20° to 2.75° are respectively as 8.8%, 26.2%, 11.2%, 5.4%, and 5.1%. Since the difference in the value of ΔN_u, 26.2%, in the second angle increase (0.55°-1.10°) is much higher than those in the other angle increases, the angle of 1.10° can be chosen as the optimised angle for these kinds of the columns. Conclusively, the value of ΔN_u equal to 35% for 1.10° angle increase can be selected as the optimised enhancement. This value corresponds to ΔA_s = 0.210 and ΔV_c = 0.532.

5. Conclusions

Structural behaviour of the TCFSC columns subjected to eccentric loading has been investigated in this paper. The proposed finite element modelling using LUSAS software was verified by comparison of the modelling result with the existing experimental test result. It was concluded that the modelling in this study can predict the structural behaviour of the columns with a sufficient accuracy. Nonlinear finite element analyses were conducted to study effects of various variables such as different tapered angles, steel wall thicknesses, load eccentricities, L/H ratios, concrete compressive strengths and steel yield stresses on the structural behaviour of the columns. According to the results of this study, these variables have considerable effects on the behaviour of the columns. The enhancement of the steel wall thickness and/or tapered angle of the columns improves the ultimate load capacity, ductility and stiffness of the columns. Also, increasing the load eccentricity has an adverse affect on the ultimate load capacity. Furthermore, enhancing the concrete compressive strength and/or steel yield stress increases the ultimate load capacity of the columns. The enhancement of the L/H ratio results in the increase of ductility and the decrease of the ultimate load capacity and stiffness of the columns. The tapered angle of 1.10° was chosen as the optimised angle for these columns. Since it was shown that these TCFSC columns have the advantage of high ultimate load capacity, they can be utilised in buildings where columns are subjected to large loads. On the other hand, because it was demonstrated that the TCFSC columns possess the benefit of good ductility performance, they can be used in high seismic zones where ductility of the structures is a big concern. In addition, the special appearance of these TCFSC columns due to the increase of the tapered angle from their top and bottom to their mid-height can make these columns as a good architectural choice for buildings.

References

Bahrami, A., Wan Badaruzzaman, W.H. and Osman, S.A. (2011), "Nonlinear analysis of concrete-filled steel composite columns subjected to axial loading", *Struct. Eng. Mech.,* **39**(3), 383-398.

Dabaon, M., El-Khoriby, S., El-Boghdadi, M. and Hassanein, M.F. (2009), "Confinement effect of stiffened and unstiffened concrete-filled stainless steel tubular stub columns", *J. Constr. Steel Res*., **65**(8-9), 1846-1854.

Dai, X. and Lam, D. (2010), "Numerical modelling of the axial compressive behaviour of short concrete-filled elliptical steel columns", *J. Constr. Steel Res*., **66**(7), 931-942.

Ellobody, E. and Young, B. (2006a), "Design and behaviour of concrete-filled cold-formed stainless steel tube columns", *J. Eng. Struct.*, **28**(5), 716-728.

Ellobody, E. and Young, B. (2006b), "Nonlinear analysis of concrete-filled steel SHS and RHS columns", *Thin Wall. Struct.*, **44**(8), 919-930.

Ellobody, E., Young, B. and Lam, D. (2006), "Behaviour of normal and high strength concrete-filled compact steel tube circular stub columns", *J. Constr. Steel Res.,* **62**(7), 706-715.

Furlong, R.W. (1968), "Design of steel-encased concrete beam-columns", *J. Struct. Div. ASC*E, **94**(1), 267-281.

Giakoumelis, G. and Lam, D. (2004), "Axial capacity of circular concrete-filled tube columns", *J. Constr. Steel. Res.*, **60**(7), 1049-1068.

Han, L.H. (2007), "Concrete filled steel tubular columns-Theory and practice", *2nd edition, Beijin*, Science Press, (in Chinese).

Han, L.H. and Yao, G.H. (2003), "Behaviour of concrete-filled hollow structural steel (HSS) columns with preload on the steel tubes", *J. Constr. Steel Res.*, **59**(12), 1455-1475.

Han, L.H., Ren, Q.X. and Li, W. (2010), "Tests on inclined, tapered and STS concrete-filled steel tubular (CFST) stub columns", *J. Constr. Steel Res.,* **66**(10), 1186-1195.

Han, L.H., Ren, Q.X. and Li, W. (2011), "Tests on stub stainless steel-concrete-carbon steel double-skin tubular

(DST) columns", *J. Constr. Steel Res.*, **67**(3), 437-452.
Hu, H.T. and Schnobrich, W.C. (1989), "Constitutive modeling of concrete by using nonassociated plasticity", *J. Mater. Civil Eng.*, **1**(4), 199-216.
Hu, H.T., Huang, C.S. and Chen, Z.L. (2005), "Finite element analysis of CFT columns subjected to an axial compressive force and bending moment in combination", *J. Constr. Steel Res.*, **61**(12), 1692-1712.
Hu, H.T., Huang, C.S., Wu, M.H. and Wu, Y.M. (2003), "Nonlinear analysis of axially loaded concrete-filled tube columns with confinement effect", *J. Struct. Eng.-ASCE*, **129**(10), 1322-1329.
Huang, C.S., Yeh, Y.K., Liu, G.Y., Hu, H.T., Tsai, K.C., Weng, Y.T., Wang, S.H. and Wu, M.H. (2002), "Axial load behavior of stiffened concrete-filled steel columns", *J. Struct. Eng.-ASCE*, **128**(9), 1222-1230.
Huang, Y.S., Long, Y.L. and Cai, J. (2008), "Ultimate strength of rectangular concrete-filled steel tubular (CFT) stub columns under axial compression", *Steel Compos. Struct.*, **8**(2), 115-128.
Lam, D. and Gardner, L. (2008), "Structural design of stainless steel concrete filled columns", *J. Constr. Steel Res.*, **64**(11), 1275-1282.
Liu, D. (2004), "Behaviour of high strength rectangular concrete-filled steel hollow section columns under eccentric loading", *Thin Wall. Struct.*, **42**(12), 1631-1644.
Liu, D. (2006), "Behaviour of eccentrically loaded high-strength rectangular concrete-filled steel tubular columns", *J. Constr. Steel Res.*, **62**(8), 839-846.
Liu, D. and Gho, W.M. (2005), "Axial load behaviour of high-strength rectangular concrete-filled steel tubular stub columns", *Thin Wall. Struct.*, **43**(8), 1131-1142.
LUSAS Standard User's Manual, (2006), Version 14, Kingston upon Thames, Surrey, UK.
Mander, J.B., Priestley, M.J.N. and Park, R. (1988), "Theoretical stress-strain model for confined concrete", *J. Struct. Eng.-ASCE*, **114**(8), 1804-1826.
Mursi, M. and Uy, B. (2003), "Strength of concrete filled steel box columns incorporating interaction buckling", *J. Struct. Eng.-ASCE*, **129**(5), 626-639.
Petrus, C., Hamid, H.A., Ibrahim, A. and Parke, G. (2010), "Experimental behaviour of concrete filled thin walled steel tubes with tab stiffeners", *J. Constr. Steel Res.*, **66**(7), 915-922.
Richart, F.E., Brandzaeg, A. and Brown, R.L. (1928), *A study of the failure of concrete under combined compressive stresses*, Bull. 185. Champaign, IL, USA: University of Illinois Engineering Experimental Station.
Saenz, L.P. (1964), Discussion of "Equation for the stress-strain curve of concrete" by Desayi, P. and Krishnan, S., *J. Am. Concrete Inst.*, **61**, 1229-1235.
Starossek, U., Falah, N. and Lohning, T. (2010), "Numerical analyses of the force transfer in concrete-filled steel tube columns", *Struct. Eng.-Mech.*, **35**(2), 241-256.
Tao, Z. and Han, L.H. (2007), "Behaviour of fire-exposed concrete-filled steel tubular beam columns repaired with CFRP wraps", *Thin Wall. Struct.*, **45**(1), 63-67.
Tao, Z., Han, L.H. and Wang, D.Y. (2007), "Experimental behaviour of concrete-filled stiffened thin-walled steel tubular columns", *Thin Wall. Struct.*, **45**(5), 517-527.
Tao, Z., Uy, B., Han, L.H. and Wang, Z.B. (2009), "Analysis and design of concrete-filled stiffened thin-walled steel tubular columns under axial compression", *Thin Wall. Struct.*, **47**(12), 1544-1556.
Tomii, M. (1991), "Ductile and strong columns composed of steel tube infilled concrete and longitudinal steel bars", Special volume, *Proceedings of the third international conference on steel-concrete composite structures*, Fukuoka, Japan: Association of Steel-Concrete Structures.
Uy, B. (1998a), "Concrete-filled fabricated steel box columns for multistorey buildings: behaviour and design", *Prog. Struct. Eng. Mater.*, **1**(2), 150-158.
Uy, B. (1998b), "Ductility, strength and stability of concrete-filled fabricated steel box columns for tall buildings", *Struct. Des. Tall Build.*, **7**(2), 113-133.
Uy, B., Tao, Z., Liao, F.Y. and Han, L.H. (2009), "Behaviour of slender square concrete-filled stainless steel columns subject to axial load", *Proceedings of the 11th Nordic steel construction conference*, held in Malmo, Sweden.
Yang, Y.F. and Han, L.H. (2009), "Experiments on rectangular concrete-filled steel tubes loaded axially on a partially stressed cross-sectional area", *J. Constr. Steel Res.*, **65**(8-9), 1617-1630.
Zhong, S.T. (1995), "Concrete-filled steel tubular structures", *Hei Lung Jiang Technology Publication Co.*, China (in Chinese).

NB